J Nanostruct 14(2): 533-547, Spring 2024

RESEARCH PAPER

Enhanced Catalytic Performance of Pt-$La_2CuFe_2O_7$/Polyaniline-Chitosan Nanocomposites for Methanol Electro-Oxidation

Somaye Khammarnia [1], Mehri-Saddat Ekrami-Kakhki [2], Jilla Saffari [3], Alireza Akbari [1]*

[1] *Chemistry Department, Payame Noor University, Tehran, 19395-4697, Iran*

[2] *Esfarayen University of Technology, Esfarayen, North Khorasan, Iran*

[3] *Department of Chemistry, Zahedan Branch, Islamic Azad University, Zahedan, Iran*

ARTICLE INFO

Article History:
Received 11 January 2024
Accepted 24 March 2024
Published 01 April 2024

Keywords:
Chitosan
Co-precipitation
Methanol Electro-oxidation
Nano-composite
Polyaniline

ABSTRACT

In this research, the $La_2CuFe_2O_7$ (LCuFO) nano-composites were synthesized by adopting the coprecipitation method. The $La_2CuFe_2O_7$ nano-composites were identified via X-ray powder diffraction (XRD) and Energy-dispersive X-ray spectroscopy (EDX). Polyaniline and chitosan (PANI-CHS) were employed as an effective and suitable substrate for these nano-composites. The Pt-LCuFO/PANI-CHS nano-composite was prepared by the chemical reduction of hexachloroplatinic acid by sodium tetrahydroborate in the presence of LCuFO nano-composite on the PANI-CHS support and it was characterized by performing TEM. Electrochemical impedance spectroscopy (EIS), chronoamperometry (CA), and cyclic voltammetry (CV) of the catalytic performance of the Pt-LCuFO/PANI-CHS nano-composite were determined for carrying out the electrooxidation of methanol via the CO stripping voltammetry. Also, the durability of the Pt-LCuFO/PANI-CHS nanocatalyst as well as the effect of multiple factors, including methanol concentration, temperature, and scanning speed were investigated for the electrooxidation of methanol. The increased catalytic performance of Pt-LCuFO/PANI-CHS nano-catalyst in comparison with the Pt/PANI-CHS suggests its application for the electrooxidation of methanol in direct methanol fuel cells.

How to cite this article
Khammarnia S., Ekrami-Kakhki M., Saffari J. Akbari A. Enhanced Catalytic Performance of Pt-$La_2CuFe_2O_7$/Polyaniline-Chitosan Nanocomposites for Methanol Electro-Oxidation. J Nanostruct, 2024; 14(2):533-547. DOI: 10.22052/JNS.2024.02.015

INTRODUCTION

In the past decades, fuel cells have attracted considerable attention as energy converters with high efficiency and low/zero emissions due to high energy demand, fossil fuel depletion, as well as environmental pollution. At the current technological stage, in addition to the expense, reliability as well as stability problems, the main challenge to the hydrogen gas fuel cells is the production, storage, and transportation of hydrogen. Direct methanol fuel cells (DMFCs) using liquid methanol as fuel are promising candidates in terms of fuel feed strategies and consumption. DMFCs use liquid methanol fuel which is easy to transport and store and simplify the fuel cell systems. However, hydrogen-powered fuel cells possess low capacity or a modifier unit in hydrogen storage tanks [1]. DMFCs have outstanding properties, including low operating temperature, easy fluid handling, as well as high energy density,

* *Corresponding Author Email: somayekhammarnia@pnu.ac.ir*

which make them promising candidates for the power supply of portable electronic devices. Although a lot of studies have been conducted on this area, DMFCs have several problems that must be addressed regarding efficiency as well as power density.

Pt has a high catalytic activity (hereafter referred to as CAL) for methanol oxidation (MO) at low temperatures below 100 °C. However, it is poisoned by carbon monoxide (CO), which is produced as a MO byproduct and deactivates the Pt surface [2]. Utilizing methanol as a fuel has many advantages over hydrogen. For instance, methanol is easy to transport and store and it is a cost-effective liquid fuel with high theoretical energy density. Moreover, since the process of MO is a slow reaction, a number of active sites are required to adsorb methanol and donate OH species to remove the residual byproducts of MO. Since the early 1970s, researchers have thoroughly investigated methanol oxidation, especially the recognition of reaction intermediates, the modification of the Pt surface as well as the poisoning species and products to achieve better resistance to poisoning and higher activity at lower potentials. Several authors have investigated the results. Although considerable amounts of methyl formate, formic acid, and formaldehyde were identified, the major product was the CO_2 reaction. Further research shows that the reaction can be based on mechanisms. However, it is commonly accepted that due to this simple reaction mechanism, the most important reactions are methanol uptake and CO oxidation. Pt is a very active metal for adsorbing the methanol decomposer. However, CO can easily poison Pt at room or medium temperature [3]. Although DMFCs are proposed as promising sources of energy because of their high conversion energy yielding, their commercialization is prevented by barriers including the low kinetics of methanol electro-oxidation as well as the penetration of methanol into the proton exchange membrane. There is a general agreement that the key reason for the slow kinetics of MO is the CO species produced during MO. The most commonly accepted strategy for the prevention of CO poisoning is utilizing Pt/metal oxide composites or Pt-based alloys according to the electronic effect and functional mechanism [4]. Good environmental resistance, inexpensive production in large amounts, easy control and synthesis are properties which have made polyaniline commercially attractive. However, this material is easily used as foam. Thin film is not made with good mechanical properties, so its application is limited in practice. In this regard, many efforts have been put into making polyaniline composites with better processing ability as well as mechanical properties while preserving the polymer conductivity. Recently, mixtures containing a conductive polymer and a hydrogel have attracted considerable attention because they can produce electrically active hydrogels capable of physical or chemical transfer in response to electrical potentials. As a result, researchers have investigated the combination of these two materials for use in controlled drug release and biosensors. Examples of hydrogel/conductive polymer mixtures include polypyrrole/poly (2-hydroxyethyl methacrylate), polypyrrole/polyacrylamide, and polypyrrole/polyacrylic. As a copolymer of 2-amino-2-deoxy-D-glucopyranose and 2-acetamide-2-deoxy-D-glucopyranose, chitosan has an interconnected styrene polymer with hydrogel-like properties by using glutaraldehyde as one of the cross-linking agents. Chitosan in the form of hydrogels has many uses such as separation membrane, wastewater treatment, food packaging, wound healing, and drug delivery systems [5]. Conducting chitosan (CHS)/polymer composites have represented good properties for different types of applications as conductive and biocompatible materials. Composites are made by incorporating a rigid conductive polymer (e.g., PANI) into a flexible matrix (e.g., CHS) by combining good matrix processing and the electrical conductivity of a conductive polymer. In addition, conductive polymers are capable of efficiently transferring electrical charges generated through a biochemical reaction to an electronic circuit. Biosensors made using a conductive polymer as a support material have operational stability, high storage, and fast response time. Polyaniline has been widely investigated due to its electrochemical, chemical, optical and electrical properties. In addition, it is resistant in air and has an easy synthesis method. However, impenetrability and solubility in common organic solvents are the main drawbacks of PANI. One of the feasible methods to prepare soluble PANI is through substituted groups [6]. Perovskites with the formula ABO_3 (A = rare earth metals, and B = intermediate metal) are used as a suitable catalytic material in processes such as

the oxidation of alcohols [7-9]. In recent years, perovskites with the chemical composition of $ABO_{3-\delta}$ (A = Ba, Ce, Sr, and La and B = Ce, Fe, Pd, Pt) and with outstanding electrical conductivity have been considered as promising candidates for direct methanol fuel cell anodes [10].

Within this research work, LCuFO nanoparticles were synthesized. The novel Pt-LCuFO/PANI-CHS nanocomposite was prepared through the chemical reduction of hexachloroplatinic acid in the presence of LCuFO nanoparticles in polyaniline (PANI) and chitosan (CHS) substrates. The catalytic activity of the novel Pt-LCuFO/PANI-CHS nanocomposite was investigated for methanol oxidation for the first time and compared with that of Pt/PANI-CHS. The electrochemical investigations were performed through different electrochemical techniques, for example cyclic voltammetry (CV), and electrochemical impedance spectroscopy (EIS). The results demonstrated that the CAL of the Pt-LCuFO/PANI-CHS nanocatalyst for MO was better than that of the Pt/PANI-CHS nanocatalyst.

MATERIAL AND METHODS

Fe $(NO_3).9H_2O$, $LaCL_3.7H_2O$ (98%), $CuCl_2.6H_2O$, NaOH and octanoic acid from Merck were utilized for synthesizing LaCuFO nanocatalyst. Hexachloroplatinic acid and sodium tetrahydroborate were bought from Merck and used for preparing Pt nanoparticles. Polyaniline was prepared from Sigma Aldrich. Chitosan was bought from Fluka and used as a substrate for the preparation of Pt-LCuFO/PANI-CHS nanocomposite. Sulfuric acid (98% mercury) was used as an electrolyte. The solution of acetic acid 1% (glacial, 100% Merck) was utilized for preparing CHS solution. Moreover, methanol (99.2%) was purchased from Merck and its oxidation was studied.

Preparation of LCuFO nanocatalyst

To prepare LCuFO nanocatalyst, solutions were prepared by dissolving 0.0111 mol (1.542 g) of $LaCl_3.7H_2O$, 0.11 mol (4.484 g) of $Fe(NO_3)_3.9H_2O$ and 0.0055 mol (0.740g) of $CuCl_2.6H_2O$ separately in 10 ml of distilled water. Next, the three solutions were mixed together. Then, 2 ml of octanoic acid was added to the solution and stirred vigorously. Afterwards, its pH reached 9 by using sodium hydroxide 5M. The precipitate was washed and

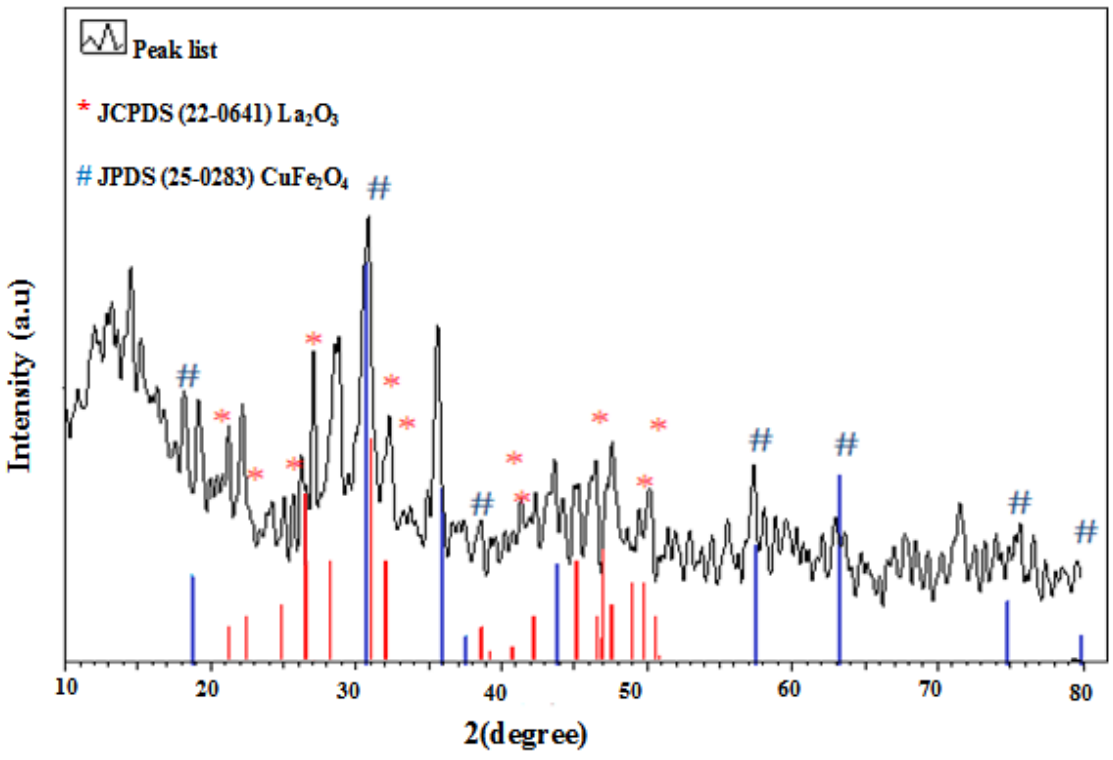

Fig. 1. XRD pattern of $La_2CuFe_2O_7$ nanocomposite.

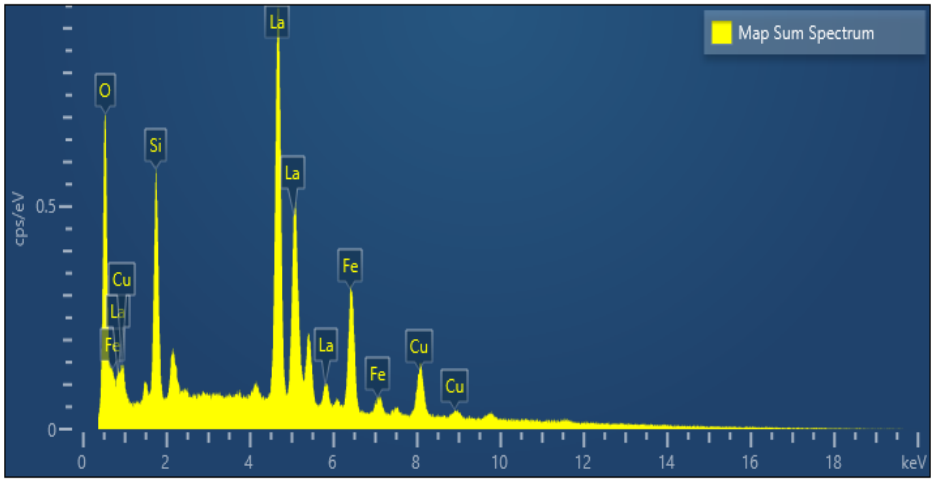

Map Sum Spectrum							
Element	Line Type	Weight %	Weight % Sigma	Atomic %	Oxide	Oxide %	Oxide % Sigma
O	K series	23.80	0.16	60.55			
Si	K series	9.38	0.12	13.59	SiO2	20.07	0.25
Fe	K series	9.66	0.14	7.04	FeO	12.43	0.18
Cu	K series	5.96	0.17	3.82	CuO	7.46	0.21
La	L series	51.20	0.23	15.00	La2O3	60.05	0.27
Total		100.00		100.00		100.00	

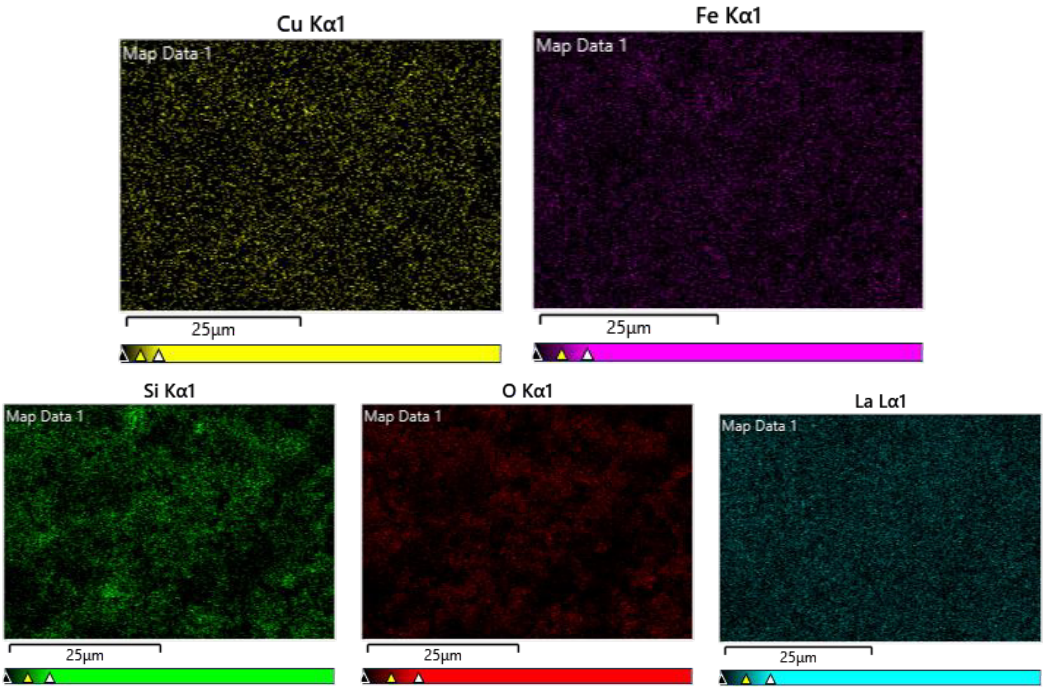

Fig. 2. EDX spectra of $La_2CuFe_2O_7$ nanocomposite materials indicate the presence of different elements in accordance with the synthetic compositions.

dried at room temperature. The powder was calcined at 800 ºC for 4 h. The LCuFO nanocatalyst was synthesized and identified.

Synthesis of Pt-LCuFO/PANI-CHS nanocomposite

To prepare Pt-LCuFO/PANI-CHS nanocatalyst, first 1 mg of polyaniline was dissolved in a

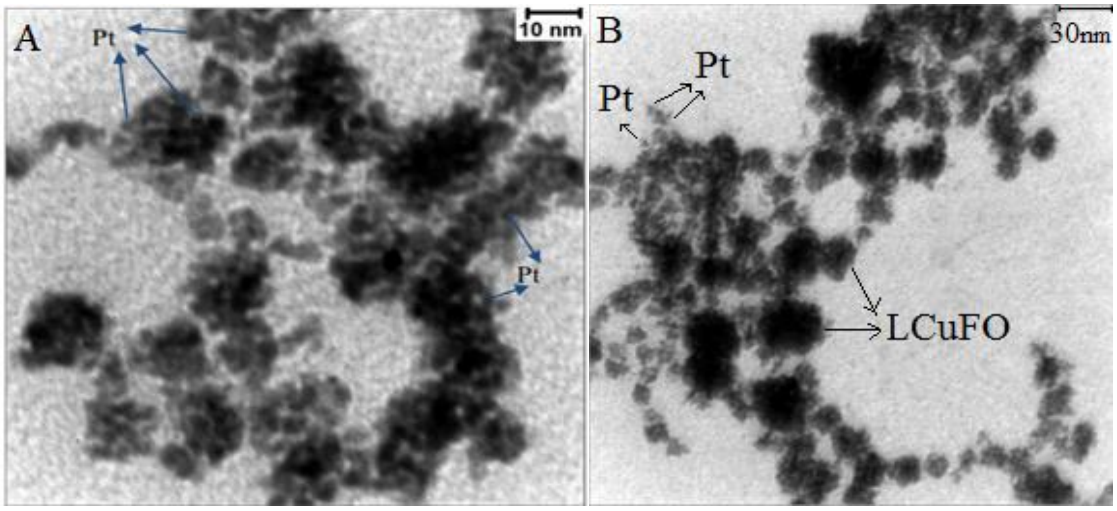

Fig. 3. TEM images of A) Pt/PANI-CHS and B) Pt-LCuFO/PANI-CHS catalysts.

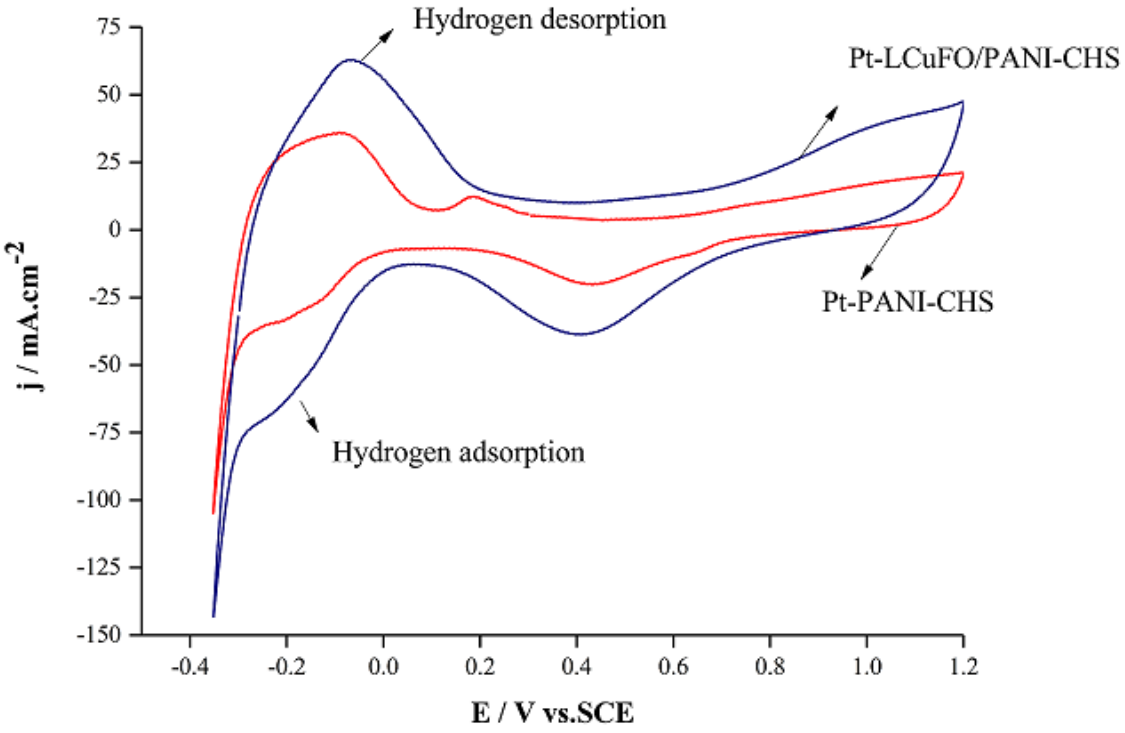

Fig. 4. CV curves of Pt/PANI-CHS and Pt-LCuFO/PANI-CHS catalysts in H_2SO_4 0.5 M solution.

mixture of ion-free water and chitosan (7: 1 ratio). After increasing 2 mg of LCuFO catalyst, ultrasonication was performed for 1 hour. Then, 25 µl of hexachloroplatinic acid 1M was added to the solution and stirred for one hour. Later, 50 µl of sodium tetrahydroborate 5M was added to the mixture. After stirring for 24 hours, the resulting mixture was centrifuged and washed several times with ion-free water. The Pt-LCuFO/PANI-CHS nanocatalyst was prepared after drying the mixture for 12 h at 60 ºC. The Pt/PANI-CHS nanocatalyst was prepared using the similar method without using the LCuFO nanoparticles.

Preparation of the electrodes

In order to prepare the modified GC/Pt/PANI-CHS and GC/Pt-LCuFO/PANI-CHS electrodes, 2 mg of the corresponding catalyst powder was added to 1 ml of CHS solution and sonicated for ten minutes. Then, 5 µl of the corresponding suspension was placed on the surface of the glassy carbon electrodes and dried at room temperature.

Characterization

The appearance and size of the nanoparticles were determined through transmission electron microscope (TEM) images with the resolution of 2.5 Å. The structure of nanocatalysts was characterized by XRD (model Philips PC-APD with CuKα radiation (λ = 1/5406 Å)). The electrochemical studies were performed using Autolab potentiostat device (Nova software, model PGSTAT 302N, Metrohm, Netherlands). A three-electrode cell was utilized. Glassy carbon electrodes (GC) with 2 mm diameter were used as the working electrode. Pt electrodes were used as auxiliary and saturated calomel electrodes (SCE) were used as reference electrodes.

RESULTS AND DISCUSSION

Catalyst characterization

The prepared LaCuFeO nanocatalyst was identified by X-ray diffraction technique. The structural characterization of nanoparticles was performed by X-ray diffraction device (XRD)

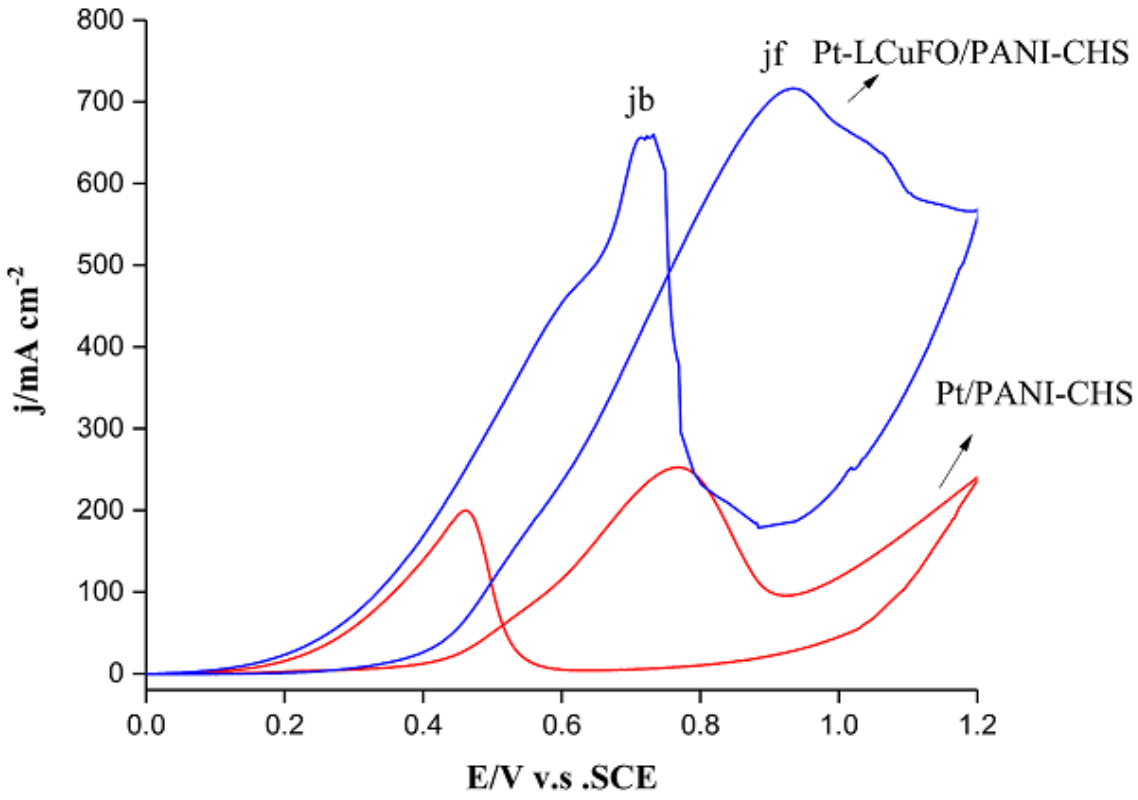

Fig. 5. CV curves of Pt/PANI-CHS and Pt-LCuFO/PANI-CHS catalysts in 0.5 M H_2SO_4 and 1.68 M methanol.

model Philips PC-APD with radiation CuKα (λ =1.5406Å). The X-ray diffraction pattern of LCuFO nanoparticles was demonstrated in Fig. 1. With the combination of standard $CuFe_2O_4$ (25-0283) with cubic symmetry, the network parameters were: a = 8.3490, a = 8.3490 and b = 34.890, and with the combination of standard La_2O_3 (22-0641) with monoclinic symmetry, the network parameters were: a = 14.60000Å , b=3.71700Å, and c=9.27800 Åperfectly matched. It was found that the value of the crystallite size did not change substantially with the nature of transition metal, 8.7 and 13.03 nm for La_2O_3 in $La_2CuFe_2O_7$ and $CuFe_2O_4$ respectively. EDX studies (Fig. 2, labeled) confirmed the presence of La, O, Fe and Cu in the catalysts depending upon the compositions and verified their presence in agreement with the experimental feed. A small Si signal was observed in the synthetic compositions due to the sample stub used in EDX analysis. The size, shape and distribution of Pt-LCuFO/PANI-CHS and Pt/PANI-CHS nanocatalyst were demonstrated with TEM images in Fig. 3. As shown in Fig. 3, Pt nanoparticles and LCuFO nanocomposites have a uniform distribution in the polyaniline and chitosan substrates. The TEM image of the Pt/PANI-CHS nanocatalyst demonstrated that the

Table 1 The electrochemical data of methanol electrooxidation at different catalysts.

Catalysts	EAS ($m^2\ g^{-1}_{Pt}$)	E_f (V) vs. SCE	j_f ($mA\ mg^{-1}_{Pt}$)	ref
Pt/PVA-CuO-Co_3O_4/CH	54.56	0.810	3010.86	[14]
Pt/PVA-CuO-Co_3O_4	35.89	0.744	1597.984	[14]
Pt/PA-CH	54.69	0.766	4967.561	[15]
Pt-LFO/PA-CH	77.46	0.793	9209.268	[15]
Pt-NFO/PA-CH	94.46	0.932	15755	[16]
Pt/LP-TiO_2/CFP	230.04	0.7	1182.8	[17]
PtPdCr/C	65	0.69	969	[18]
Pt-C/Fe_2-CoP	117.34	0.7	1237	[19]
Pt-$FeNi_2P$/C	90.47	0.641	1125	[20]
Pt/C-Au@CeO_2-Pt	77.8	0.8	1267	[21]
Commercial Pt/C	45.6	0.7	616	[21]
Commercial Pt/C (20% Pt)	65.7	0.65	258.5	[22]
Pt NPs/C	22	0.65	153.8	[23]
Pt NWs/NL-CNS	115.9	0.7	1949.5	[23]
Pt/C (C:Vulcan carbon)	39.67	0.62	192.97	[24]
Pt/OMCS (ordered mesoporous carbon sphere)	73.5	0.9 vs. NHE	510	[25]
Pt/Bnt-CH	133.41	0.854	4316.67	[26]
Pt/Bnt-mRGO-CH	138.502	0.891	4189.107	[26]
Pt/PANI-CHS	54.69	0.724	6151.341	This work
Pt-LCuFO/PANI-CHS	145.64	0.927	17426.24	This work

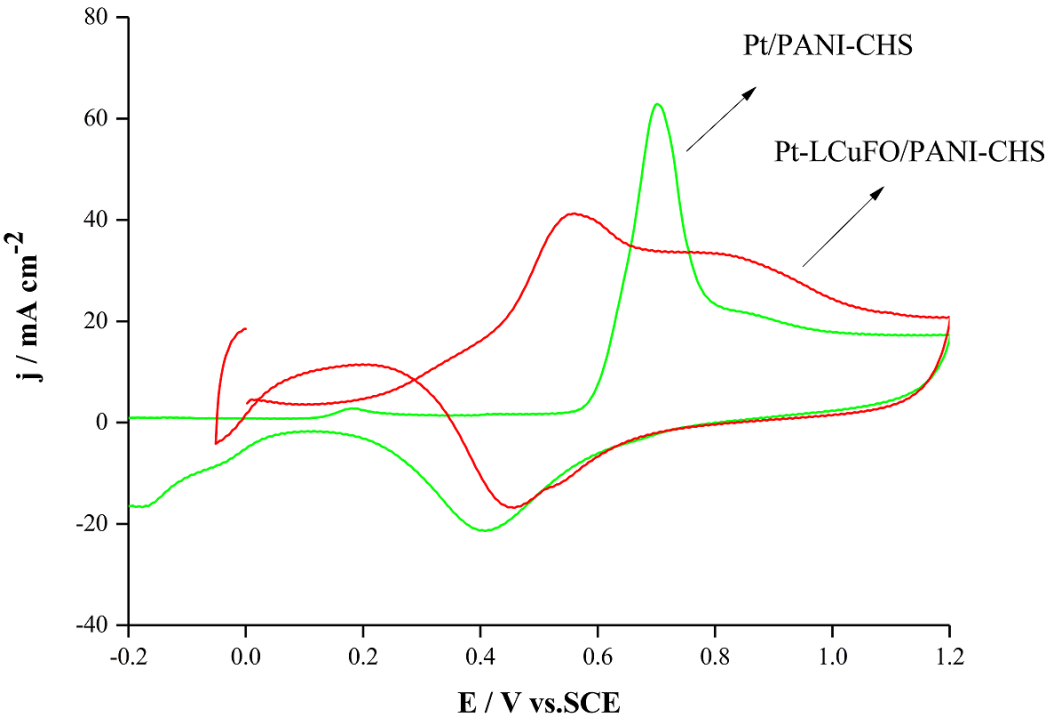

Fig. 6. CO oxidation curves of Pt/PANI-CHS and Pt-LCuFO/PANI-CHS catalysts in H_2SO_4 0.5 M solution.

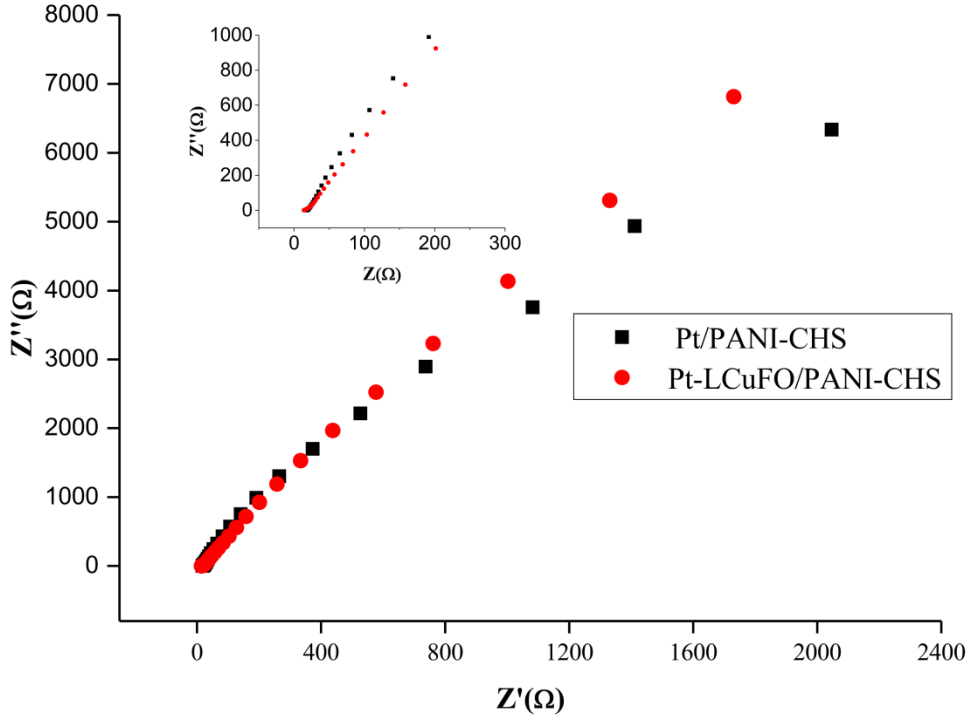

Fig. 7 Nyquist plots of Pt/PANI-CHS and Pt-LCuFO/PANI-CHS catalysts in 0.5 M H_2SO_4 and 1.68 M methanol.

average size of Pt nanoparticles was around 2.63 nm. Also, the TEM image of Pt-LCuFO/PANI-CHS nanocatalyst showed that the mean sizes of Pt and LCuFO nanoparticles were approximately about 2.63 nm and 17.66 nm, respectively.

Electrocatalytic measurements

Fig. 4 demonstrates the electrochemical behavior of Pt/PANI-CHS and Pt-LCuFO/PANI-CHS in 0.5 M sulfuric acid solution. The electrochemically active surface area (EAS) were obtained by measuring the hydrogen adsorption and desorption charges in 0.5 M sulfuric acid solution and using equation (1) [11].

$$EAS = \frac{Q_H}{0.21 \times [Pt]} \quad (1)$$

In this equation, Q_H signifies the coulomb charge for adsorption and desorption of hydrogen and 0.21 mC cm^{-2} is needed for hydrogen monolayers to be adsorbed on the surface of Pt nanoparticles. The amount of Pt loaded on the surface of the glassy carbon electrode [Pt] was specified by optical emission spectroscopy of the conjugated plasma [12].

With the uniform loading of Pt nanoparticles, electrochemically active surface area value for Pt-LCuFO/PANI-CHS catalyst (145.64 m^2g^{-1}) was much higher than that of Pt/PANI-CHS catalyst (54.69 m^2g^{-1}) which indicates that the CAL of Pt-LCuFO/PANI-CHS catalyst for MO is significantly higher than Pt/PANI-CHS and it has more active sites for MO.

The CAL of Pt/PANI-CHS and Pt-LCuFO/PANI-CHS nanocatalysts for methanol electrooxidation was studied and demonstrated in Fig. 5. The synthesized catalysts exhibited two oxidation peaks for methanol electrooxidation. The first anodic peak (j_f) in the forward sweep was related to methanol electrooxidation and the second oxidation peak (j_b) was related to the oxidation of the intermediates produced during MO in the reverse scan [13].

At LCuFO/PANI-CHS and Pt/PANI-CHS nanocatalysts, the first peak of MO was observed at 0.927 and 0.764 V, respectively. The second MO peak was observed in the reverse scan at 0.724 and 0.460 V, respectively. The anodic peak current density of MO at Pt-LCuFO/PANI-CHS catalyst was 714.476 mA cm^{-2}, which was significantly higher than that of Pt/PANI-CHS catalyst (252.205 mA cm^{-2}). The better catalytic activity of Pt-LFO/

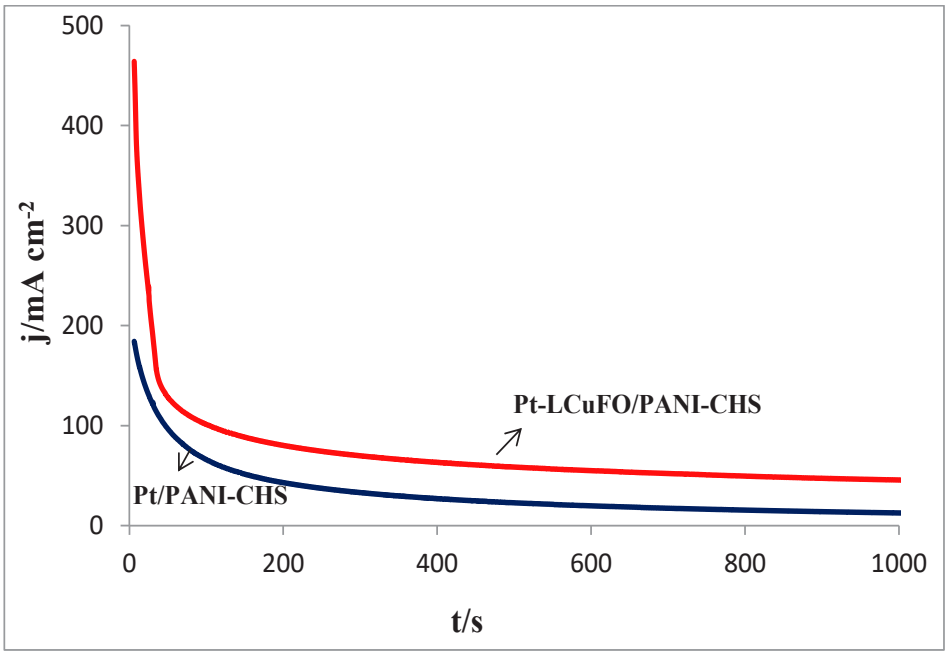

Fig. 8. Chronoamperometry curves of Pt/PANI-CHS and Pt-LCuFO/PANI-CHS catalysts in 0.5 M H_2SO_4 and 1.68 M methanol.

PANI-CHS nanocatalyst for MO was ascribed to the presence of LFO nanoparticles accompanied by platinum nanoparticles. The electrochemical data of methanol electrooxidation at different catalysts was represented in Table 1. CO stripping voltammetry was used to determine the CO-poisoning resistance of Pt-LCuFO/PANI-CHS and Pt/PANI-CHS nanocatalysts and demonstrated in Fig. 6. [27]. To conduct the CO stripping experiment, the CO gas was entered into the H_2SO_4 0.5 M solution while the constant potential of 0.2 V was applied for 20 min. N_2 was then bubbled for 20 min for removing the unabsorbed CO gas [28]. The initial potential for the oxidation of the adsorbed CO onto Pt/PANI-CHS was 0.574 V and it was 0.2 V for Pt-LCuFO/PANI-CHS. The CO oxidation peak of Pt-LCuFO/PANI-CHS was observed at 0.554V. However, the CO oxidation peak of Pt/PANI-CHS was observed at 0.701 V. The peak and onset potentials for the oxidation of the adsorbed CO onto Pt-LCuFO/PANI-CHS nanocatalyst was significantly lower in comparison with that of Pt/PANI-CHS nanocatalyst, indicating that the adsorbed CO on Pt-LCuFO/PANI-CHS surface was oxidized and removed more easily, compared to that of Pt/PANI-CHS. Therefore, the CO tolerance of Pt/LCuFO/PANI-CHS was higher in comparison with that of Pt/PANI-CHS [29, 30].

The behavior of Pt/PANI-CHS and Pt-LCuFO/PANI-CHS for methanol electrooxidation was investigated through EIS. EIS studies were performed using Nyquist curves [31] in the range of 1×10^{-3} to 1×10^{-2} Hz at open circuit potential in 0.5 M acid and 1.68 M methanol solution (Fig. 7). In the Nyquist curves of the synthesized catalysts, there was a very small semicircle and a line in the high frequency and low frequency regions, respectively, which were ascribed to the process of charge transport process at the interface between the electrode and the electrolyte and the diffusion process in the synthesized catalysts, respectively. As illustrated in Fig. 7, the Pt-LCuFO/PANI-CHS catalyst has a smaller semicircle diameter and a more vertical straight line than Pt/PANI-CHS. Therefore, it shows the faster kinetics of Pt-LCuFO/PANI-CHS catalyst for ion diffusion process and faster charge transport reaction of this nanocatalyst in comparison with Pt/PANI-CHS for methanol electrooxidation [32].

The chronoamperometry (CA) technique was

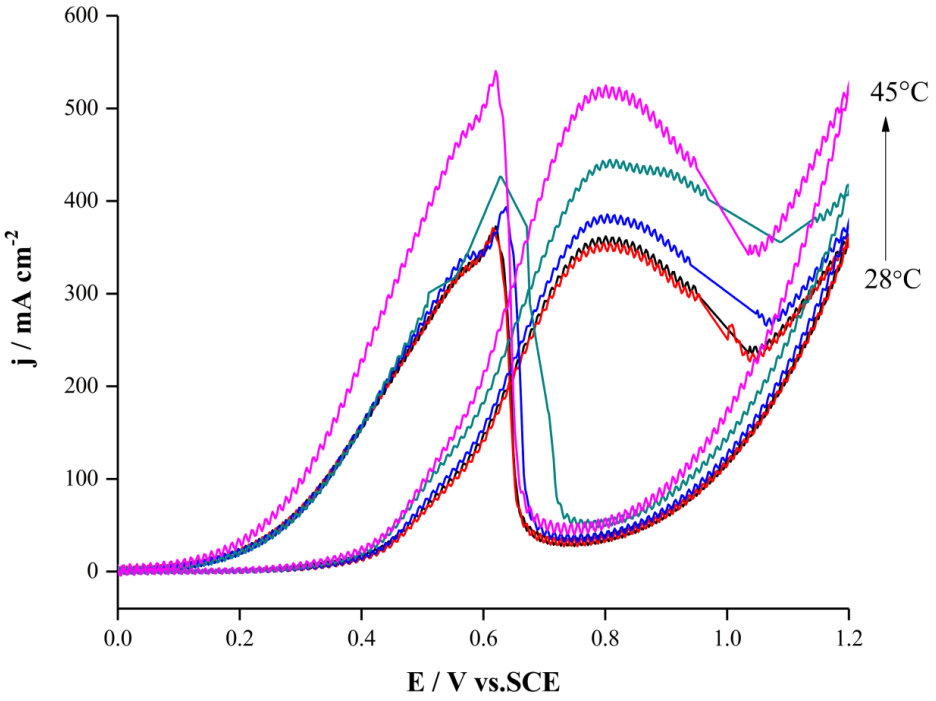

Fig. 9 CV curves of Pt-LCuFO/PANI-CHS catalyst at various temperatures of 28, 30, 35, 40, and 45 ˚C in 0.5 M H_2SO_4 and 1.68 M methanol.

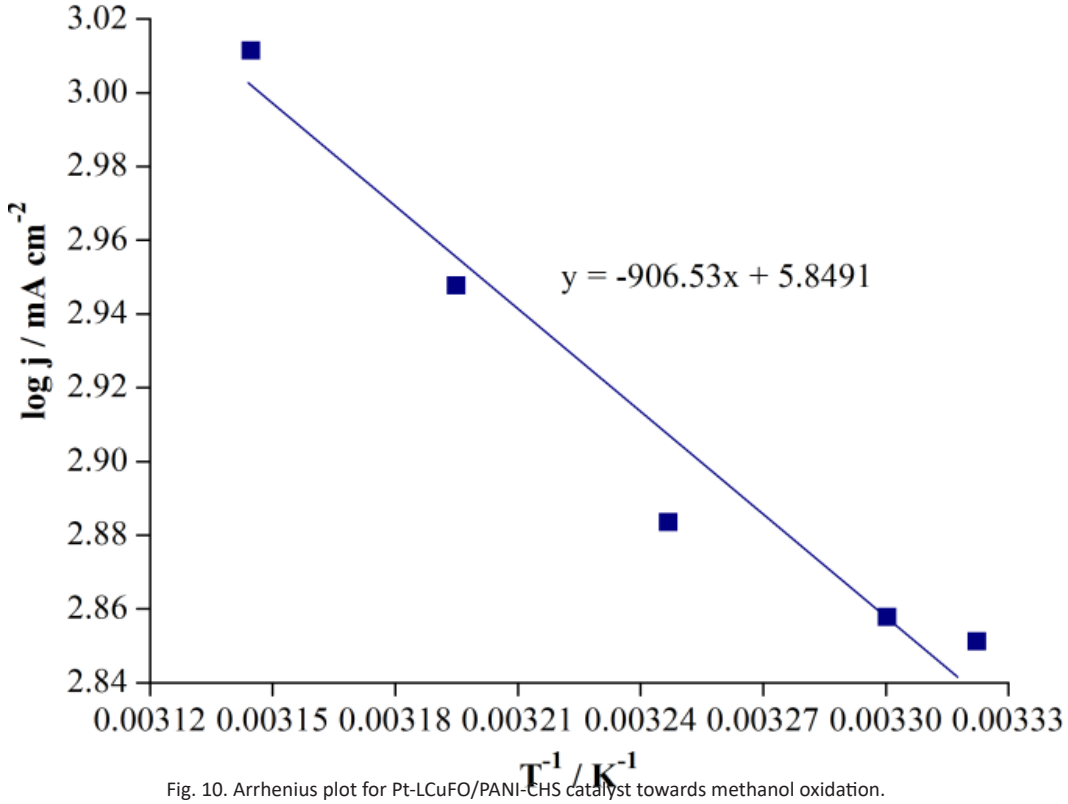

Fig. 10. Arrhenius plot for Pt-LCuFO/PANI-CHS catalyst towards methanol oxidation.

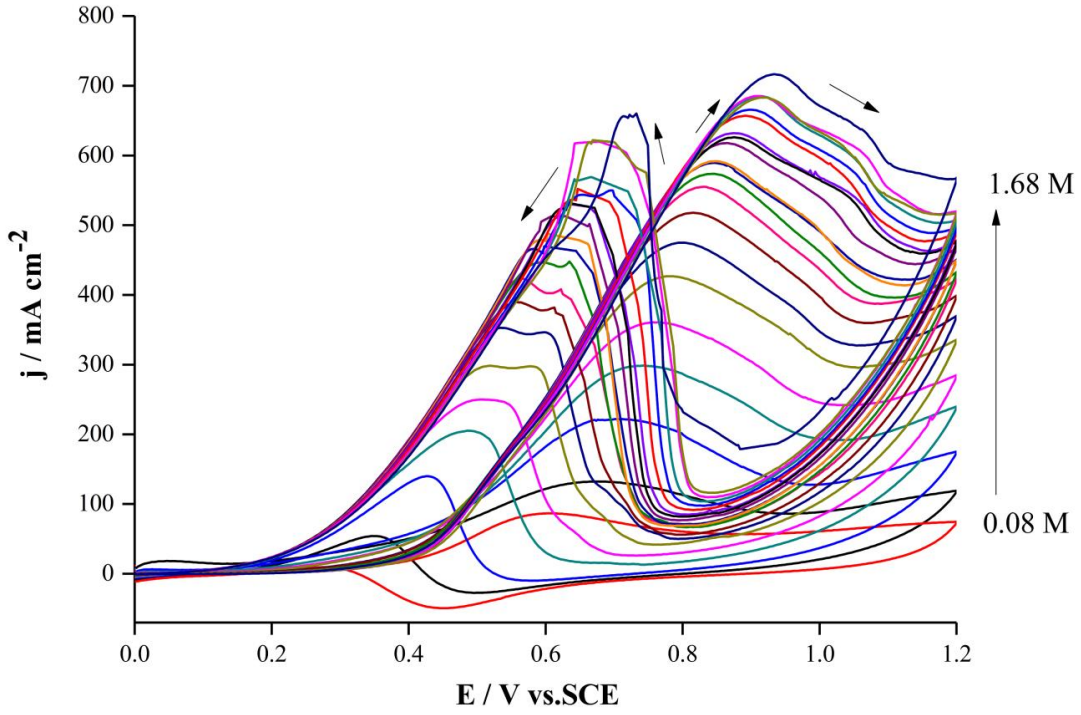

Fig. 11. CV curves of MO at Pt-LCuFO/PANI-CHS catalyst in 0.5 M H_2SO_4 and various concentrations of methanol: 0.08, 0.16, 0.24, 0.32, 0.41,0.48, 0.56, 0.64, 0.72, 0.79, 0.88, 0.96, 1.04, 1.12, 1.20, 1.28, 1.36, 1.44, 1.52, 1.6, 1.68 M.

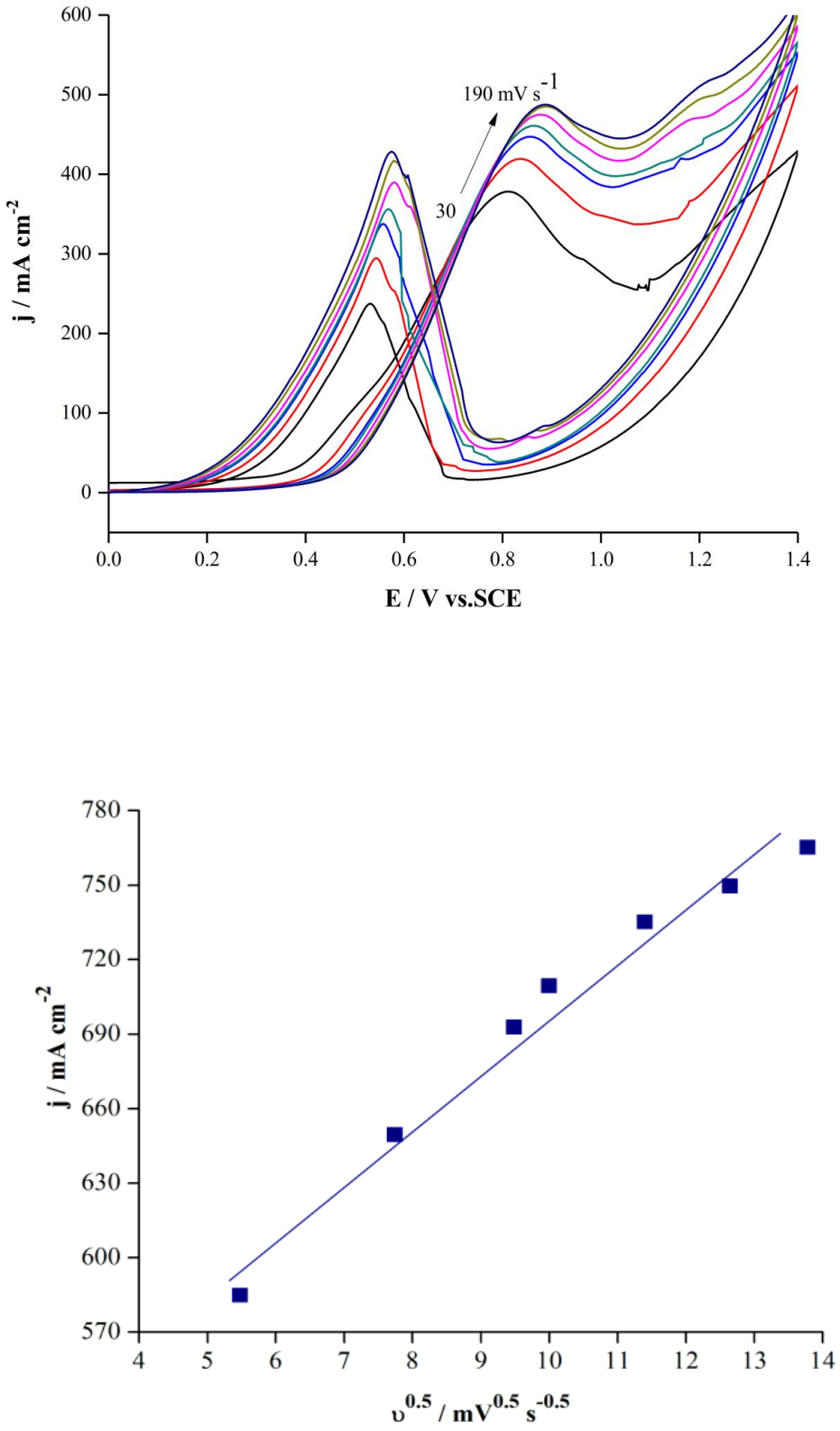

Fig. 12. CV curves of MO at Pt-LCuFO/PANI-CHS catalysts at different scan rates (30, 60, 90, 100, 130, 160, and 190 mV s^{-1}) in 1.68 M methanol and 0.5 M H_2SO_4. The anodic peak current density (jf) vs. square root of scan rate ($\upsilon^{0.5}$).

adopted to measure the long-term stability of Pt-LCuFO/PANI-CHS and Pt/PANI-CHS catalysts for MO reaction. The CA curves were obtained at 0.8 V vs. SCE for 1000 s in 1.68 M methanol and 0.5 M H_2SO_4. As shown in Fig. 8, the CA of Pt-NFO/PANI-CHS was better in comparison with the CA of Pt/PANI-CHS for the electrooxidation of methanol. At first, the current of the prepared catalysts reduced rapidly, which was presumably due to the intermediates produced during the MO [33]. At first, the anodic current density (ACD) of Pt-LCuFO/PANI-CHS (463.13 $mA.cm^{-2}$) was higher, compared to that of Pt/PANI-CHS (184.25 $mA.cm^{-2}$). After the measured time (1000 s), the anodic current density of Pt-LCuFO/PANI-CHS (45.85 $mA.cm^{-2}$) was still higher (around 2.8 times) than that of Pt/PANI-CHS (13.67 $mA.cm^{-2}$), demonstrating its higher tolerance against the produced intermediates (e.g. CO) during MO [34], which verified the increased CA of Pt-LCuFO/PANI-CHS in comparison with Pt/PANI-CHS for MO.

Factors affecting MO

Various factors affect the catalytic performance of Pt-LCuFO/PANI-CHS for methanol electrooxidation including temperature, methanol concentration, and scan rate. These factors were studied and optimized. The CA of Pt-LCuFO/PANI-CHS nanocatalyst was studied for methanol electrooxidation at various temperatures from 25 to 45 ˚C at 100 mV s^{-1}scan rate. As shown in Fig. 9, as the temperature increases, the anodic peak of MO rises. This indicates that at higher temperatures, Pt-LCuFO/PANI-CHS catalyst structure has active sites that are more available to perform MO reaction [35-37]. As the temperature increases from 25 to 45 ° C, the anodic peak current density increases from 709.87to 1026.78 mA cm^{-2}. The anodic peak activation energy of MO at Pt-LCuFO/PANI-CHS catalyst was also calculated using the Equation 2 and through the Arrhenius logarithm curve of the anodic peak current density log j versus of T^{-1} qshown in Fig. 10.

$$\frac{\partial \ln j}{\partial [\frac{1}{T}]} = \frac{\Delta H^*}{R} \quad (2)$$

In this equation j signifies the anodic peak current density, ΔH* signifies the activation energy, R signifies the gas constant and T signifies the temperature. The anodic peak activation energy

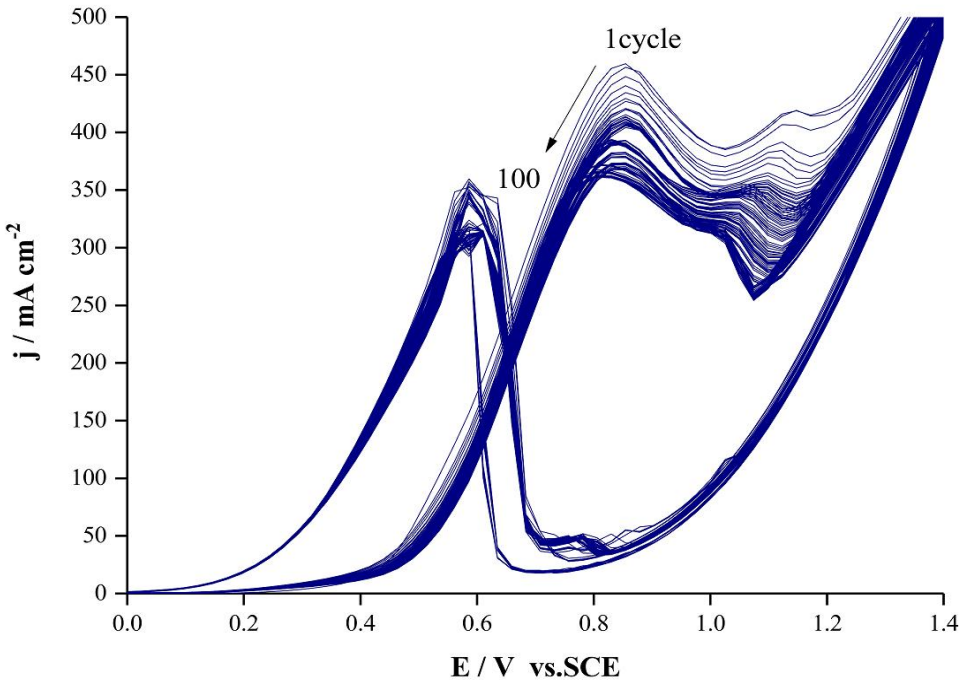

Fig. 13. CV curve Pt-LCuFO/PANI-CHS catalysts during 100 cycles in 1.68 M methanol and 0.5 M H_{2SO4} solution.

of MO at Pt-LFO/PANI-CHS catalyst was obtained 7.536 kJ mol^{-1}.

At different concentrations of methanol, the catalytic activity of the Pt-LCuFO/PANI-CHS was studied and demonstrated in Fig. 11. As the methanol concentration increases from 0.08 to 1.68 M, the peak current density of MO increases from 86.08 to 715.72 $mAcm^{-2}$. At concentrations of methanol greater than 1.68 M, the anodic current density did not change much. This was probably because the active MO sites on the electrode surface were saturated [11]. The anodic peak potential of MO changes from 0.885 to 0.913 V with increasing the concentration of methanol, which is because of the increase in platinum catalyst toxicity [38].

The CAL of the Pt-LCuFO/PANI-CHS catalyst for MO at various scan rates from 30 to190 mV s^{-1} in sulfuric acid 0.5 M was studied and demonstrated in Fig. 12. There was a rise in ACD of MO with increasing the scan rate, and there was a linear relationship between the ACD (j_f) and the root of the scan rate ($\upsilon^{0.5}$), indicating that methanol penetrates from the electrolyte solution to the surface. The Pt-LFO/PANI-CHS electrode controlled the MO reaction [39].

The effect of Pt-LCuFO/PANI-CHS catalyst poisoning on MO was investigated using cyclic voltammetry at 100 mV s^{-1} and 100 consecutive cycles (Fig. 13). In the first scan cycle at Pt-LCuFO/PANI-CHS electrode, the ACD was 712.39 mA cm^{-2} and after 100 consecutive cycles, its value reached 561.45 mA cm^{-2}. After 100 consecutive cycles, there was no considerable reduction in the amount of MO peak current density; therefore the Pt-LCuFO/PANI-CHS catalyst has good stability and durability for MO.

CONCLUSION

In this study, Pt-LCuFO/PANI-CHS nanocatalysts were successfully synthesized by dispersing LCuFO nanocomposites accompanied by platinum nanoparticles in the matrix of polyaniline and chitosan substrates. Afterwards, its CAL was identified for MO and compared with that of Pt/PANI-CHS nanocatalyst. The Pt-LCuFO/PANI-CHS nanocatalysts showed an excellent CAL for MO. It was shown that the presence of LCuFO nanoparticles along with platinum significantly increased its CAL for MO. Pt-LCuFO/PANI-CHS nanocatalyst had higher electrochemical active surface area, much higher ACD, and lower poisoning effect in contrast to Pt/PANI-CHS indicating that Pt-LCuFO/PANI-CHS is a suitable catalyst for use in DMFCs.

ACKNOWLEDGMENTS

The current study was technically and financially supported by the Islamic Azad University of Zahedan, Esfarayen University of Technology, and Payame Noor University of Mashhad.

CONFLICT OF INTEREST

The authors declare that there are no conflicts of interest regarding this article.

REFERENCES

1. Liu H, Song C, Zhang L, Zhang J, Wang H, Wilkinson DP. A review of anode catalysis in the direct methanol fuel cell. J Power Sources. 2006;155(2):95-110.
2. Choi J-H, Park K-W, Kwon B-K, Sung Y-E. Methanol Oxidation on Pt/Ru, Pt/Ni, and Pt/Ru/Ni Anode Electrocatalysts at Different Temperatures for DMFCs. J Electrochem Soc. 2003;150(7):A973.
3. Antolini E, Salgado JRC, Gonzalez ER. The methanol oxidation reaction on platinum alloys with the first row transition metals. Applied Catalysis B: Environmental. 2006;63(1-2):137-149.
4. Wang J, Xi J, Bai Y, Shen Y, Sun J, Chen L, et al. Structural designing of Pt-CeO_2/CNTs for methanol electro-oxidation. J Power Sources. 2007;164(2):555-560.
5. Thanpitcha T, Sirivat A, Jamieson AM, Rujiravanit R. Preparation and characterization of polyaniline/chitosan blend film. Carbohydr Polym. 2006;64(4):560-568.
6. Yavuz AG, Uygun A, Bhethanabotla VR. Preparation of substituted polyaniline/chitosan composites by in situ electropolymerization and their application to glucose sensing. Carbohydr Polym. 2010;81(3):712-719.
7. Arakawa T, Ohara N, Kurachi H, Shiokawa J. Catalytic oxidation of methanol on $LnCoO_3$ (Ln = La-Eu) perovskite oxides. Journal of Colloid and Interface Science. 1985;108(2):407-410.
8. Ekrami-Kakhki M-S, Farzaneh N, Fathi E. Superior electrocatalytic activity of Pt $SrCoO_3$–δ nanoparticles supported on functionalized reduced graphene oxide-chitosan for ethanol oxidation. Int J Hydrogen Energy. 2017;42(33):21131-21145.
9. Noroozifar M, Khorasani-Motlagh M, Ekrami-Kakhki M-S, Khaleghian-Moghadam R. Enhanced electrocatalytic properties of Pt–chitosan nanocomposite for direct methanol fuel cell by $LaFeO_3$ and carbon nanotube. J Power Sources. 2014;248:130-139.
10. Yu H-C, Fung K-Z, Guo T-C, Chang W-L. Syntheses of perovskite oxides nanoparticles $La_{1-x}Sr_xMO_{3-\delta}$ (M = Co and Cu) as anode electrocatalyst for direct methanol fuel cell. Electrochimica Acta. 2004;50(2-3):811-816.
11. Kakaei K, Rahimi A, Husseindoost S, Hamidi M, Javan H, Balavandi A. Fabrication of Pt–CeO2 nanoparticles supported sulfonated reduced graphene oxide as an efficient electrocatalyst for ethanol oxidation. Int J Hydrogen Energy. 2016;41(6):3861-3869.

12. Ekrami-Kakhki M-S, Farzaneh N, Abbasi S, Makiabadi B. Electrocatalytic activity of Pt nanoparticles supported on novel functionalized reduced graphene oxide-chitosan for methanol electrooxidation. Journal of Materials Science: Materials in Electronics. 2017;28(17):12373-12382.
13. Noroozifar M, Khorasani-Motlagh M, Khaleghian-Moghadam R, Ekrami-Kakhki M-S, Shahraki M. Incorporation effect of nanosized perovskite $LaFe_{0.7}Co_{0.3}O_3$ on the electrochemical activity of Pt nanoparticles-multi walled carbon nanotube composite toward methanol oxidation. J Solid State Chem. 2013;201:41-47.
14. Ekrami-Kakhki M-S, Naeimi A, Donyagard F. Pt nanoparticles supported on a novel electrospun polyvinyl alcohol-CuO Co_3O_4/chitosan based on Sesbania sesban plant as an electrocatalyst for direct methanol fuel cells. Int J Hydrogen Energy. 2019;44(3):1671-1685.
15. Gosavi PV, Biniwale RB. Catalytic preferential oxidation of carbon monoxide over platinum supported on lanthanum ferrite–ceria catalysts for cleaning of hydrogen. J Power Sources. 2013; 15;222:1-9.
16. Bameri I, Saffari J, Ekrami-Kakhki M-S, Baniyaghoob S. Pt Nanoparticles Incorporated $ZnFe_2O_4$ Nanoparticles Supported on Hollow Poly(aniline-co-pyrrole)/Chitosan as a Novel Catalyst for Methanol Oxidation. J Cluster Sci. 2022;34(4):1819-1829.
17. Dao DV, Adilbish G, Le TD, Nguyen TTD, Lee I-H, Yu Y-T. Au@CeO_2 nanoparticles supported Pt/C electrocatalyst to improve the removal of CO in methanol oxidation reaction. J Catal. 2019;377:589-599.
18. Xie F, Gan M, Jiang M, Ma L. Fe-doped CoP nanotube heterostructure enhanced the catalytic activity of Pt nanoparticles towards methanol oxidation reaction. Int J Hydrogen Energy. 2020;45(46):24807-24817.
19. Deng J, Zhang J, Chen J, Luo Y, Chen Y, Xue Y, et al. Fabrication of layered porous TiO_2/carbon fiber paper decorated by Pt nanoparticles using atomic layer deposition for efficient methanol electro-oxidation. J Electroanal Chem. 2020;874:114468.
20. Peng K, Bhuvanendran N, Ravichandran S, Zhang W, Ma Q, Xing L, et al. Carbon supported PtPdCr ternary alloy nanoparticles with enhanced electrocatalytic activity and durability for methanol oxidation reaction. Int J Hydrogen Energy. 2020;45(43):22752-22760.
21. Wei D, Ma L, Gan M, Han S, Shen J, Ding J, et al. Pt-based catalyst decorated by bimetallic FeNi2P with outstanding CO tolerance and catalytic activity for methanol electrooxidation. Int J Hydrogen Energy. 2020;45(7):4875-4886.
22. Zhong J-P, Hou C, Li L, Waqas M, Fan Y-J, Shen X-C, et al. A novel strategy for synthesizing Fe, N, and S tridoped graphene-supported Pt nanodendrites toward highly efficient methanol oxidation. J Catal. 2020;381:275-284.
23. Huang H, Wei Y, Yang Y, Yan M, He H, Jiang Q, et al. Controllable synthesis of grain boundary-enriched Pt nanoworms decorated on graphitic carbon nanosheets for ultrahigh methanol oxidation catalytic activity. Journal of Energy Chemistry. 2021;57:601-609.
24. Chang J, Feng L, Liu C, Xing W, Hu X. Ni2P enhances the activity and durability of the Pt anode catalyst in direct methanol fuel cells. Energy and Environmental Science. 2014;7(5):1628.
25. Zhang C-W, Xu L-B, Chen J-F. High loading Pt nanoparticles on ordered mesoporous carbon sphere arrays for highly active methanol electro-oxidation. Chin Chem Lett. 2016;27(6):832-836.
26. Aryafar A, Ekrami-Kakhki M-S, Naeimi A. Enhanced electrocatalytic activity of Pt-SnO_2 nanoparticles supported on natural bentonite-functionalized reduced graphene oxide-extracted chitosan from shrimp wastes for methanol electro-oxidation. Sci Rep. 2023;13(1).
27. Wang H, Xue Y, Zhu B, Yang J, Wang L, Tan X, et al. CeO_2 nanowires stretch-embedded in reduced graphite oxide nanocomposite support for Pt nanoparticles as potential electrocatalyst for methanol oxidation reaction. Int J Hydrogen Energy. 2017;42(32):20549-20559.
28. Alcaide F, Álvarez G, Cabot PL, Grande H-J, Miguel O, Querejeta A. Testing of carbon supported Pd–Pt electrocatalysts for methanol electrooxidation in direct methanol fuel cells. Int J Hydrogen Energy. 2011;36(7):4432-4439.
29. Feng G, Pan Z, Xu Y, Chen H, Xia G, Zhang Y, et al. Platinum decorated mesoporous titanium cobalt nitride nanorods catalyst with promising activity and CO-tolerance for methanol oxidation reaction. Int J Hydrogen Energy. 2018;43(36):17064-17068.
30. Moniri S, Van Cleve T, Linic S. Pitfalls and best practices in measurements of the electrochemical surface area of platinum-based nanostructured electro-catalysts. J Catal. 2017;345:1-10.
31. Ding K, Jia Z, Wang Q, He X, Tian N, Tong R, et al. Electrochemical behavior of the self-assembled membrane formed by calmodulin (CaM) on a Au substrate. J Electroanal Chem. 2001;513(1):67-71.
32. He Q, Chen W, Mukerjee S, Chen S, Laufek F. Carbon-supported PdM (M=Au and Sn) nanocatalysts for the electrooxidation of ethanol in high pH media. J Power Sources. 2009;187(2):298-304.
33. Zhang F, Wang Z, Xu KQ, Xia J, Liu Q, Wang Z. Highly dispersed ultrafine Pt nanoparticles on nickel-cobalt layered double hydroxide nanoarray for enhanced electrocatalytic methanol oxidation. Int J Hydrogen Energy. 2018;43(33):16302-16310.
34. Li XT, Lei H, Yang C, Zhang QB. Electrochemical fabrication of ultra-low loading Pt decorated porous nickel frameworks as efficient catalysts for methanol electrooxidation in alkaline medium. J Power Sources. 2018;396:64-72.
35. Shafaei Douk A, Saravani H, Noroozifar M. A fast method to prepare Pd-Co nanostructures decorated on graphene as excellent electrocatalyst toward formic acid oxidation. J Alloys Compd. 2018;739:882-891.
36. Yavari Z, Noroozifar M, Khorasani-Motlagh M. Multifunctional catalysts toward methanol oxidation in direct methanol fuel cell. J Appl Electrochem. 2015;45(5):439-451.
37. Ekrami-Kakhki M-S, Farzaneh N, Abbasi S, Beitollahi H, Ekrami-Kakhki SA. An Investigation of Methyl Viologen Functionalized Reduced Graphene Oxide: Chitosan as a Support for Pt Nanoparticles Towards Ethanol Electrooxidation. Electronic Materials Letters. 2018;14(5):616-628.
38. He Z, Chen J, Liu D, Zhou H, Kuang Y. Electrodeposition of Pt–Ru nanoparticles on carbon nanotubes and their electrocatalytic properties for methanol electrooxidation. Diamond Relat Mater. 2004;13(10):1764-1770.
39. Zhao Y, Wang R, Han Z, Li C, Wang Y, Chi B, et al. Electrooxidation of methanol and ethanol in acidic medium using a platinum electrode modified with lanthanum-doped tantalum oxide film. Electrochimica Acta. 2015;151:544-551.